Journal of Hydrology: Regional Studies 26 (2019) 100629

Contents lists available at ScienceDirect

Journal of Hydrology: Regional Studies

journal homepage: www.elsevier.com/locate/ejrh

Assessment of antecedent moisture condition on flood frequency: An experimental study in Napa River Basin, CA

Jungho Kim[a,b,*], Lynn Johnson[a,b], Rob Cifelli[b], Andrea Thorstensen[c], V. Chandrasekar[a]

[a] Cooperative Institute for Research in the Atmosphere (CIRA), Colorado State University, Fort Collins, CO, USA
[b] NOAA Earth System Research Laboratory, Physical Sciences Division, Boulder, CO, USA
[c] NOAA National Weather Service, North Central River Forecast Center, USA

ARTICLE INFO

Keywords:
Flood frequency
Antecedent moisture condition
Precipitation frequency
T-year flood simulation
Distributed hydrologic model
Radar-based precipitation data

ABSTRACT

Study region: This study region is the Napa River basin in California whose antecedent soil moisture states and precipitation magnitudes are primary drivers to occur extreme floods.
Study focus: This study assessed the influence of antecedent moisture condition on flood frequency, based on an experimental application scheme and pre-processing. For this purpose, T-year flood simulations were conducted using a distributed hydrologic model. Distributed precipitation patterns which have an amount of precipitation corresponding to a specific T-year return period were generated by representative radar-based precipitation fields and precipitation frequency analysis. Dry, normal, and wet of antecedent moisture condition were applied to each T-year flood simulation to reflect variable initial soil moisture states.
New hydrological insights for the region: The relationship among flood frequency, antecedent moisture condition, and precipitation frequency was derived for a specific target storm event. For normal antecedent moisture states, the relation showed that T-year precipitation could generate floods having return intervals nearly identical to those derived using gage records. For saturated soil conditions, a 7-year precipitation event could trigger a 100-year flood. Conversely, a 200-year precipitation event with dry soil conditions might generate only a 15-year flood event. The results emphasize the importance of soil moisture to flood runoff and suggest that soil-moisture monitoring could aid in improving flood forecasting.

1. Introduction

In hydrology, flood frequency (FF) analysis has been used for decades due to its applicability and utility (Katz et al., 2002). One of the major applications of FF is the prediction of proper design floods for constructing hydraulic structures such as dams, bridges, levees, culverts, highways, and sewage-disposal plants (Dalrymple, 1960). Also, knowledge of the FF is necessary to quantify and classify risk levels of a flood event in vulnerable areas. Since floods with T-year recurrence intervals are reference values to measure the intensity of flood events, FF has informed forecasters, operators, and decision makers responsible for issuing flood warnings and operating hydraulic infrastructures. For example, coupling flood forecasting to distributed hydrologic models that generate runoff outputs at any location in the domain enables prediction of flood risk levels for an entire watershed, even in ungauged regions.

The general approach of FF analysis is based on deriving FF curves by estimating the exceedance probability of annual maximum

* Corresponding author at: Cooperative Institute for Research in the Atmosphere (CIRA), Colorado State University, Fort Collins, CO, USA.
E-mail addresses: jungho.kim@noaa.gov, jungho.kim@colostate.edu (J. Kim).

https://doi.org/10.1016/j.ejrh.2019.100629
Received 30 December 2018; Received in revised form 24 June 2019; Accepted 19 September 2019
Available online 30 September 2019

flood series (Gumbel, 1941; Powell, 1943; Eagleson, 1972; England et al., 2018). Most countries including the United States use the FF methodology and have also modified the general approach to characterize uncertainty (Cameron et al., 1999; Blazkova and Beven, 2002; Brath et al., 2006; Halbert et al., 2016), regional variability (Pandey and Nguyen, 1999; De Michele and Rosso, 2001; Ouarda et al., 2001; Smith et al., 2015), climate change impacts (Cameron et al., 2000; Kay et al., 2009; Arnell and Gosling, 2016), and urbanization impacts (Hollis, 1975; Prosdocimi et al., 2015) on FF. On the other hand, there are arguments against employing general FF analysis due to wrong interpretation of FF, randomness and probability of annual maximum floods, and extrapolations of FF curves (Klemeš, 2006). Merz and Gunter (2008a; 2008b) raised up an issue that a number of intrinsic weaknesses of the flood frequency analysis mainly related to the problem that the available flood peak sample cannot be representative of behavior of potential future floods.

The continuous rainfall-runoff simulation opens up several avenues of research, notably with respect to uncertainty in estimating flood frequency and the question of consistency of model calibrations (i.e. parameterization) for both continuous flow series and flood frequency simulation (Cameron et al., 1999). If a continuous model is provided with observed rainfall data, then will one or more sets of parameters that provide acceptable rainfall-runoff simulation results could provide acceptable estimates of the flood frequency characteristics. A number of previous studies who proposed continuous rainfall-runoff simulation to estimate flood frequency showed how the continuous modeling can be used to quantify floods for spillway design (Bergstrôm et al., 1993) and under climate change (Cameron et al., 1999, 2000). Blazkova and Beven (2002) implemented the attempt at flood frequency estimation by continuous simulation to include the possibility of snowmelt and rain-on-snow flood cases. Cameron et al. (1999) well described the benefits of employing a continuous rainfall-runoff simulation for estimating flood frequency.

Although many studies have highlighted the importance of hydrological reasoning in flood frequency estimation, most publications in the hydrological literature have focused on subtleties of the estimation problem (Merz and Gunter, 2008a, 2008b). This study intends to address another issue, namely the relations between FF, antecedent moisture condition (AMC) and precipitation, and is to answer the two questions which have not been explored before: (1) Depending on the states of antecedent moisture content, what scale (i.e. flood frequency) of flooding can occur? and (2) Depending on the interactions of antecedent moisture states and precipitation magnitude, what scale of flooding can occur? Since each flood value in the annual maximum flood series used in FF analysis arises from specific precipitation and AMC conditions, we are interested in the interactions between these conditions and FF. We hypothesize that the estimating the thresholds of AMC and precipitation that generate an extreme flood return period are the most significant question in terms of flood forecasting. However, it is difficult to find reasonable answers to the question from FF analysis. This is because T-year floods only represent probabilistic flood levels by adopting T-year recurrence intervals, which themselves are based on historic flood events and are not representative of FF-AMC-precipitation relations. Thus, it is necessary to implement an assessment of AMC and precipitation on FF, to examine the variability of flood frequency in response to them.

A number of studies have reviewed the effects of AMC and precipitation on runoff flows (De Paola et al., 2013; Han et al., 2019; Osborn and Hickok, 1968; Hawkins et al., 1985; Merz and Plate, 1997; Tucker and Bras, 2000; Tramblay et al., 2010; Yoo et al., 2012; Huza et al., 2014). As precipitation is the primary source of the variability of runoff responses, precipitation magnitude must be predicted prior to a storm event. AMC also has a large effect on flood discharge as it determines a volume of direct runoff (Martínez-Mena et al., 1998; Castillo et al., 2003; Tramblay et al., 2010; Penna et al., 2011; Kim et al., 2018a; Kim et al., 2018b Chifflard et al., 2018). Many studies address the effect of AMC on runoff flows: De Michele and Salvadori (2002) analyzed the influence of AMC on flood frequency distribution and derived the distribution of peak flows conditioned by the AMC statistical law; Castillo et al. (2003) examined the effect of initial soil moisture content on runoff response in the Green-Ampt method by deploying a Monte Carlo simulation technique for different scenarios; Javelle et al. (2010) emphasized the influence of AMC in potential flood vulnerable areas.

The use of FF is highly efficient, but cannot represent interactions and contributions of AMC and precipitation to FF. The previous studies cited above reviewed the effects of AMC and precipitation on runoff, but did not investigate the relation between precipitation frequency (PF), AMC states, and FF, or the effect of the AMC-PF interactions on FF. To resolve the issues, it is needed to derive FF-AMC-PF relations and to confirm their interactions with flood discharge. It is also necessary to review the contributions of precipitation and AMC to a specific T-year return period of flood in order to estimate the thresholds of precipitation and AMC that could generate an extreme return period of flood.

The aim of this study is to assess effects of AMC on flood frequency. The assessment is implemented by using rainfall-runoff simulations with various precipitation magnitudes and AMC states. PF is used to consider various and specific precipitation magnitudes and to generate T-year precipitation data. Multi/Radar Multi/Sensor (MRMS) is used to reflect the spatial distribution of the observed precipitation field. Using MRMS data and T-year precipitation information, T-year distributed precipitation fields are generated through a simple merging approach. The NOAA Hydrology Laboratory-Research Distributed Hydrologic Model (HL-RDHM) is used as the distributed hydrologic and continuous model; it is based on the Sacramento soil moisture accounting (SAC-SMA) methodology. AMC states are estimated and classified using state variables in SAC-SMA. Finally, this study simulates T-year floods by forcing the hydrologic model with T-year distributed precipitation data and the AMC states, and diagnoses the impact of precipitation and AMC on flood frequency through analysis of total runoff flows (TRF) and peak flows. The Napa River basin in northern California is selected as an application area.

Section 2 details the distributed hydrologic model, the radar-based precipitation product, and the assessment process and pre-processing methods used. Section 3 explains the application watershed, data, and the pre-processing results which cover analyses of precipitation and flood frequency, generation of T-year distributed precipitation fields, and estimation of the states of AMC. Section 4 provides the assessment results for total runoff flows and peak flows.

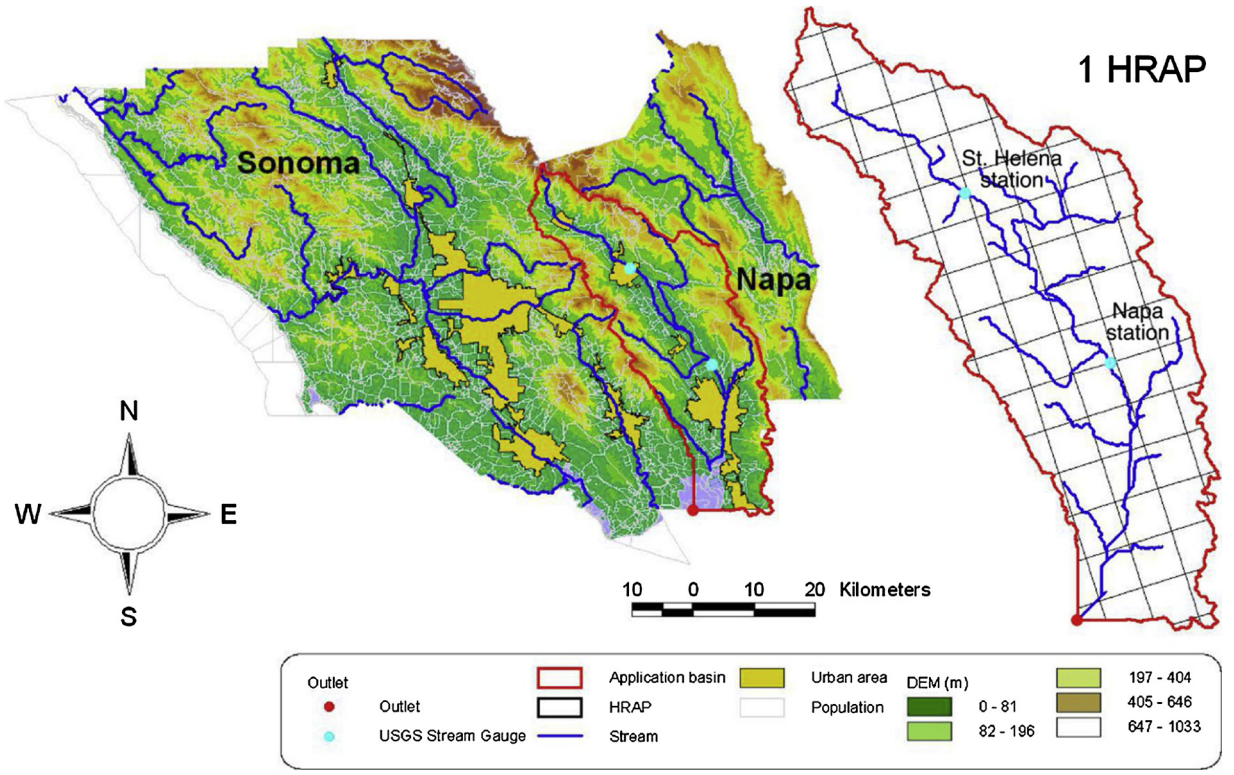

Fig. 1. Application watershed: Napa River basin with digital elevation model and channel network (left) and drainage area for hydrologic modeling based on the HRAP grid network (right).

2. Materials and methods

2.1. Application basin and data

The test basin used is the Napa River basin, located in northwestern Napa County just south of the summit of Mt. St. Helena in the Mayacamas Mountains of the California Coast Range. Fig. 1 shows the Napa River basin, showing its elevation and HRAP-grid network and drainage channel network. The Napa River begins as the seasonal Kimball Canyon Creek in Robert Louis Stevenson State Park at an elevation of 3745 feet (1141 m), which descends the southern slopes of Mt. St. Helena to Kimball Canyon Dam (Johnson et al., 2016). In 1986, the worst of 23 floods recorded since 1865 on the Napa River occurred: 5000 people were evacuated, 250 homes were destroyed, and three people lost their lives.

The Napa River basin has complex terrain with land cover dominated (65% by area) by a combination of Evergreen Forest and Grassland. This basin has two continuous flow gages managed by the U. S. Geological Survey (USGS): the upper gage is NAPA R NR ST HELENA CA station (called the “St. Helena station” herein) and the lower gage is USGS 11458000 NAPA R NR NAPA CA station (“Napa station”; Fig. 1). The Napa station was the primary site used for this study: it has a drainage area of 564.6 sq. km, over which the annual average precipitation is 703.8 mm, and of which roughly 80% occurs during a rainy season from November to March. Unfortunately, the application basin has no available monitoring system for soil moisture.

The Napa River watershed is covered by two S-band Next-Generation Radars (NEXRADs – KDAX and KMUX) operated by the National Weather Service (NWS) and KPIX radar C-band gap-filling TV station radar (i.e., KPIX). MRMS QPE products were generated using the combination of NEXRAD and KPIX radar data. In this study, gridded precipitation fields at a spatial resolution of 1.0 km and an hourly temporal resolution are used to implement the pre-processing.

Radar-based precipitation data provides a gridded precipitation field representing the spatial variability of precipitation intensity with specific resolutions (Yoo et al., 2013; Kim and Yoo, 2014; Kim et al., 2015). In the US, the Multi/Radar Multi/Sensor (MRMS) product is distinguished by its high accuracy and national consistency (Willie et al., 2016). MRMS’s automated algorithms integrate data streams from ground-based multiple radars, air observations, lightning-detection systems, and satellite- and forecast-based models. The primary purpose of the MRMS system is to produce severe weather and precipitation products for decision-making capability to improve severe weather forecasts and warnings, hydrology, aviation, and numerical weather prediction (Zhang et al., 2016).

This study used MRMS data produced by Willie et al. (2016). MRMS QPE products include radar-only, radar-only with VPR correction, and radar with VPR and gauge correction QPE, based on the availability of the relevant input data. The radar with VPR

and gauge correction QPE is used in this study since its assessment is superior to the other products.

2.2. Distributed hydrologic model

The use of a distributed hydrologic model (DHM) is an attractive alternative to hydrological process simulation for rainfall-runoff analysis and flood prediction with remote sensing inputs and geographic information systems (Krajewski et al., 1991). This study employs a DHM for simulating T-year floods because DHMs are capable of capturing the spatial distribution of meteorological input variables (e.g. precipitation) and physical parameters (e.g. soil saturation and terrain routing-related) while a lumped or semi-distributed hydrologic model is not able to (Zhang et al., 2013). Among many of the developed DHMs, the Hydrological Laboratory-Research Distributed Hydrologic Model (HL-RDHM) developed by the NOAA National Weather Service (NWS) Office of Hydrologic Development (OHD) can accurately forecast the complex water balance dynamics of watersheds (Spies et al., 2015). The HL-RDHM is a combination of physically-based and conceptual model features (Koren et al., 2004). This model consists of a conceptual water balance model (Sorooshian et al., 1993) applied on a regular spatial grid linked to physically-based kinematic hillslope and channel routing models (Chow et al., 1988). The HL-RDHM was designed and implemented for the entire contiguous United States, and can be applied for any grid resolution and time step (National Weather Service (NWS, 2011; Thorstensen et al., 2016). The HL-RDHM takes account of the spatial variability of weather variables, land-use, soils, and terrain as the model is based on the Hydrologic Rainfall Analysis Project (HRAP) grid structure, providing an efficient interface for spatially distributed inputs and hydrologic outputs (Koren et al., 2003). In contrast to traditional lumped models, advantages of the HL-RDHM include the ability to use gridded remote sensing precipitation data and to derive estimates of runoff flow and soil moisture at any location in the watershed. The HL-RDHM integrates algorithms for spatially distributed precipitation (e.g., radar-based precipitation data in HRAP), soil moisture accounting, snowmelt, and evapotranspiration, conceptual hillslope and channel routing. For more detailed descriptions of the method see NWS (2011) and Thorstensen et al. (2016).

The core of the HL-RDHM is the SAC-SMA model, which determines contributions of precipitation to the infiltrated water and runoff flow (Sorooshian et al., 1993). Fig. 2 shows the conceptual diagram of the model structure within the hydrologic cycle. The SAC-SMA model is a conceptual soil moisture accounting model consisting of tension and free water in the upper and lower zones to characterize soil moisture states and runoff components. To represent soil moisture storage and movement within each zone, the SAC-SMA has 16 parameters, including six relating to soil moisture storage capacity, three for recession, four for percolation, and the three related non-modified parameters (Thorstensen et al., 2016).

The SAC-SMA also has five states of soil moisture content that could be used as boundary conditions of AMC (ADIMC is dependent on UZTWC and LZTWC) as shown in Fig. 2. These states result from antecedent precipitation and interactions of hydrological processes (drainage, evaporation, and transpiration), with water in a soil column representing the current amount of tension and free water contents in the upper and lower zones. In the upper zone, the water content state rapidly decreases due to subsurface runoff by free water and the tension water by evaporation (or evapotranspiration). In the lower zone, free water storage is divided into two sub-storages that control supplemental flow (fast) and primary groundwater flow (slow). Between upper and lower zones, percolation is a link to supply water to a lower zone.

2.3. Application scheme and pre-processing

We establish an application scheme to implement the assessment of precipitation and AMC to FF, at the heart of which is simulating T-year floods by forcing reasonable alternatives of precipitation and AMC. The scheme includes the following steps: (1) pre-processing to generate T-year distributed precipitation and AMC states to reflect dry, normal, and wet conditions; (2) rainfall-runoff modeling to generate runoff outputs from each AMC; and (3) assessment of the combined precipitation and AMC on the runoff outputs. Fig. 3 shows the application algorithm and methods.

In the pre-processing, there are three major components, as follows: A. precipitation and flood frequency analysis; B. generation of T-year distributed precipitation fields; and C. estimation and identification of AMC states corresponding to the driest, normal, and wettest cases. To implement component A, this study adopts references that provide reasonable frequency analysis results in precipitation and runoff conditions, the details of which are described in Section 3.3.

In component B, T-year distributed precipitation fields are generated from the MRMS QPE product and T-year precipitation from the PF analysis. The PF from the first component A is used for estimating precipitation magnitudes corresponding to T-year recurrence intervals of precipitation in the application watershed. The spatial distributions of precipitation are extracted from an actual event defined as the target storm, which represents typical climatic precipitation patterns in the Napa river watershed. To seek the target storm with a spatial distribution most similar to the long-term climate precipitation pattern, MRMS QPE products are compared with PRISM climate data (http://www.prism.oregonstate.edu/) at the HRAP resolution (~ 4.0 km) from 30 years of recorded data. When comparing MRMS QPE products and PRISM climate data, the accumulated precipitation fields are used since PRISM climate data is only available for monthly values. The details of the comparison are described in session 3.1.2.

To generate T-year distributed precipitation fields, a simple merging approach is applied using the spatiotemporal distributions of the target storm and T-year precipitation. For example, if the target storm has a duration of 12 h, the specific T-year distributed precipitation in hourly time steps consists of 12 distributed precipitation fields equal to the target storm. The temporal distribution of precipitation also follows that of the target storm. The temporal distribution of the target storm is extracted using hourly areal average precipitation (AAP). The AAP is calculated from Eq. (1):

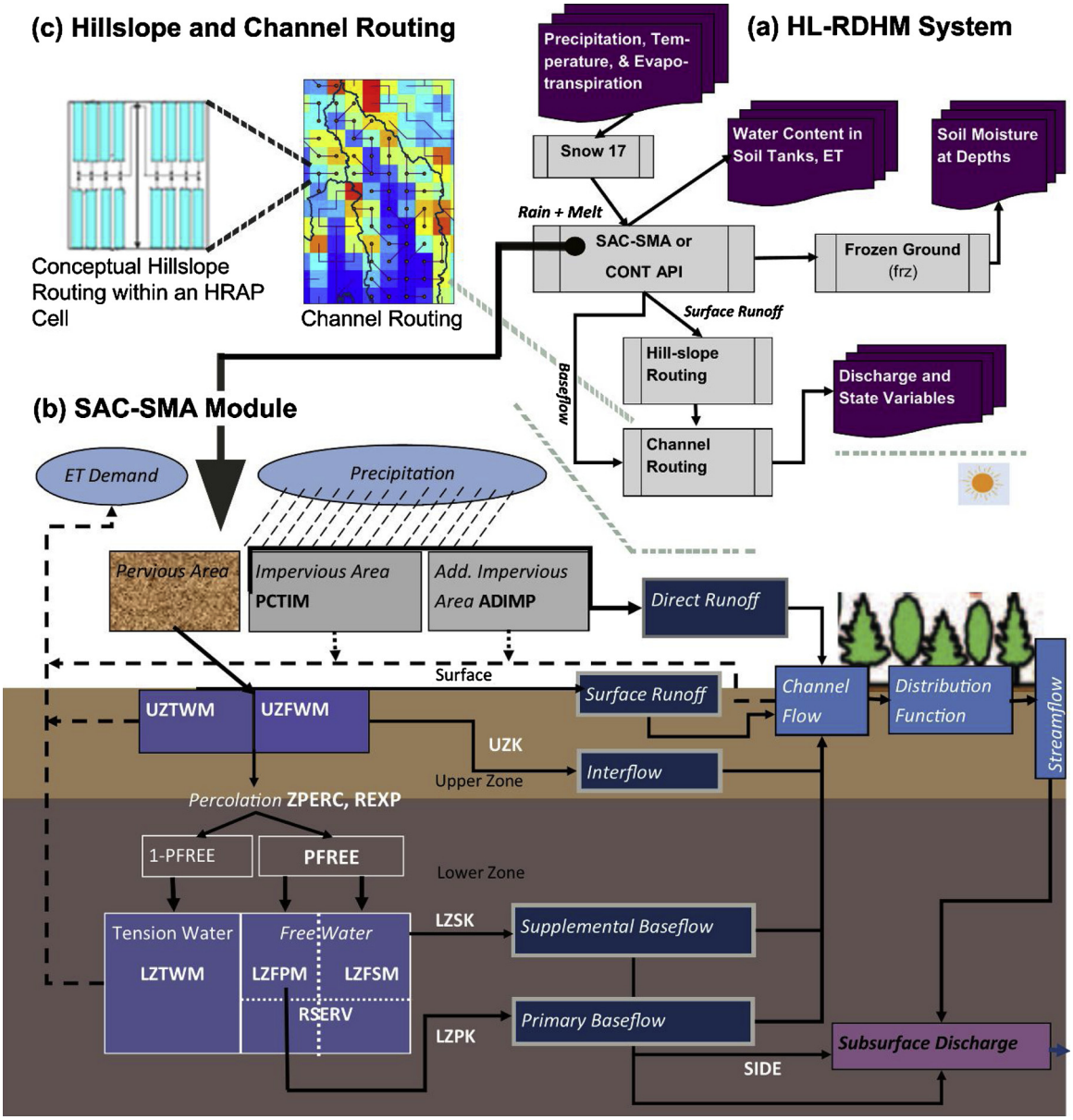

Fig. 2. Conceptual schematic for the HL-RDHM and the Sacramento soil moisture accounting process.

$$AAP(R_G(t)) = \left[\sum_{j=1}^{m}\sum_{i=1}^{n} R_G(t,i,j)\right]/(n \times m) \tag{1}$$

while the temporal distribution of T-year precipitation is resolved as that of the target storm by using Eq. (2):

$$R_F(t) = R_F \times AAP(R_G(t))/\sum_{i=1}^{duration} AAP(R_G(i)) \tag{2}$$

where *AAP* is the areal average precipitation, $R_G(t)$ is the gridded precipitation field (e.g., MRMS QPE products) at time *t*, $R_G(t,i,j)$ is each value in the gridded precipitation field, and *n* and *m* are row and column numbers. $R_F(t)$ is the temporally resolved hourly T-year precipitation, R_F is T-year precipitation corresponding to a specific recurrence interval.

The merging approach for distributed precipitation fields (using MRMS QPE products) and T-year precipitation is implemented using scale factors to match the hourly precipitation amount of the distributed precipitation fields with the hourly T-year precipitation temporally resolved. In this process, the scale factor is calculated from Eq. (3) for each time step (*t*) and at each grid (*i, j*) of MRMS QPE data. From Eq. (3), MRMS QPE fields at each *t* are normalized using the *AAP* value for whole girds. The MRMS QPE fields

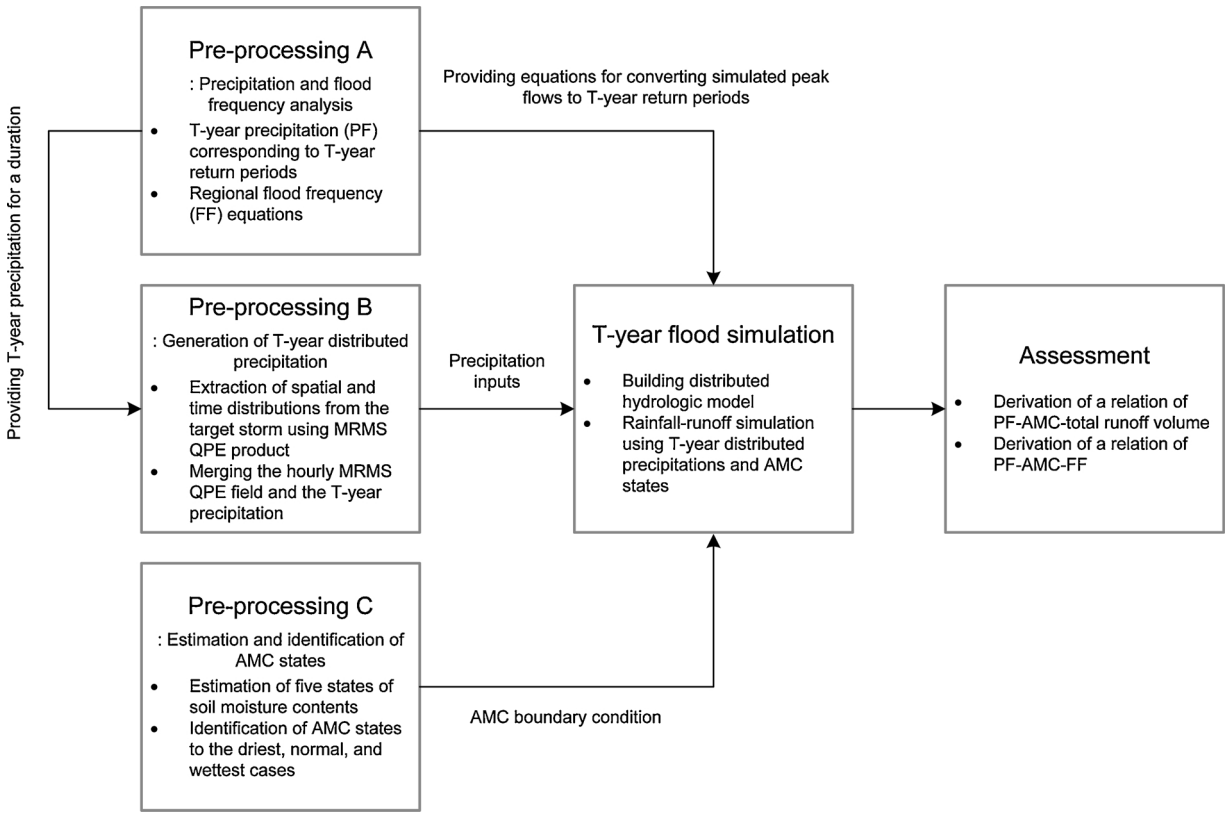

Fig. 3. Diagram of the application process in this study.

are then scaled up by multiplying the scale-factor to the normalized MRMS QPE field through Eq. (4). Thus, the areal average value of the scaled-up precipitation field equals that of the temporally resolved hourly T-year precipitation at the same *t*. Through this final step, T-year distributed precipitation can be generated for the duration of a target storm.

$$F_{scale}(t, i, j) = R_G(t, i, j)/AAP(R_G(t)) \tag{3}$$

$$R_{FG}(t, i, j) = R_F(t) \times F_{scale}(t, i, j) \tag{4}$$

In Eq. (3), F_{scale} is scale factor for each grid value at time *t*. $R_{FG}(t,i,j)$ in Eq. (4) is each grid value in T-year distributed precipitation fields.

In the component C of the pre-processing, the states of AMC are estimated for a variety of soil moisture boundary conditions to the T-year flood simulations. Five states of soil moisture content in SAC-SMC model are used as indices representing the AMC states with free and tension waters in the upper and lower zones. Many sets of the five states comprising the AMCs are estimated by simulating multiple storm events, and then AMC states are classified as either driest, normal, or wettest conditions.

In the T-year flood simulation process, The HL-RDHM for the application watershed is established and calibrated, and T-year flood simulations are implemented by forcing the HL-RDHM model with the generated T-year distributed precipitation and the estimated states of AMC. Total Runoff Flows (TRF) in depth and peak flows are used to conduct the assessment, and the relations of TRF-AMC-PF and FF-AMC-PF are derived. In addition, this application scheme is specified to smaller watersheds whose AMC states and precipitation magnitudes are primary drivers to occur extreme floods. Also, it has no upstream regulation and no effects of snow on streamflows.

Detailed results of the processing described above is addressed in Section 3.1. It contains results of hydrological modeling, generated T-year distributed precipitation fields, and estimated antecedent moisture content states.

2.4. Precipitation and flood frequency

This study employed NOAA Atlas 14 developed by the Hydrometeorological Design Studies Center within the Office of Hydrologic Development of the NOAA's National Weather Service (Perica et al., 2014). We selected a range of return periods from 2 to 200 years for a length of 12 h since the target storm has a 12 -h duration. For the duration of 12 h, the drainage area for the Saint Helena station has T-year precipitation areal average depths ranging from 69.1 mm (2-year) to 150.6 mm (200-year), whole those at Napa station range from 50.3 mm to 130.3 mm.

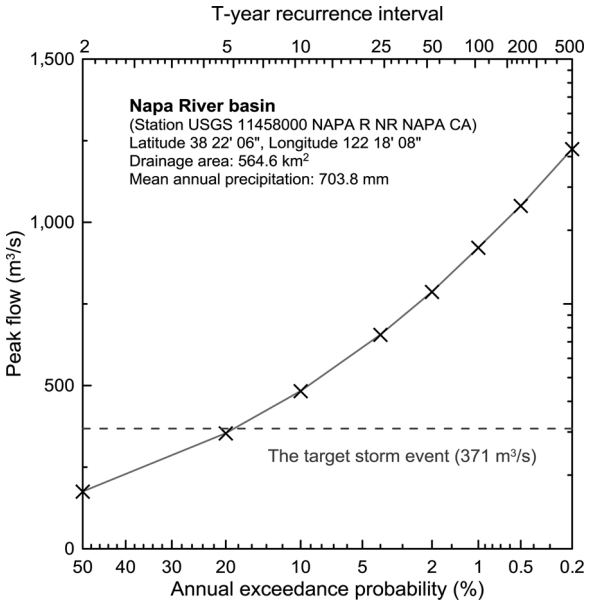

Fig. 4. Flood frequency curve with peak flows and annual exceedance probabilities corresponding to T-year recurrence intervals in the USGS station 11458000.

This study employed regional flood frequency equations from Gotvald et al. (2012), who implemented regional regression analysis using generalized least squares regression to develop a set of equations with 50-, 20-, 10-, 4-, 2-, 1-, 0.5-, and 0.2-percent annual exceedance probabilities. The analysis was predicated on the availability of at least 10 years of annual peak flow data and that peak flows were not substantially affected by diversions or urbanization. The flood frequency equation in Gotvald et al. (2012) has two parameters, drainage area and average annual precipitation. Fig. 4 shows the estimated peak flows corresponding to T-year recurrence intervals at the Napa station. The range is from 175 to 1224 m^3/s for 2 ~ 500 year recurrence intervals.

$$T - year\ return\ period\ =\ exp\,(0.005269 \times simulated\ peakflow) \times 0.785 \quad (5)$$

In addition, an equation to convert simulated peak flows to T-year return periods is required in this study. Thus, this study derived the equation resulting from regression analysis using the exponential function as shown below in Eq. (5). Since the R-squared value for the regression equation is above 0.98, the equation was deemed acceptable to convert the simulated peak flows to T-year return periods for deriving the relation of PF, AMC, and FF.

3. Results

3.1. Pre-processing results for T-year flood simulations

3.1.1. Hydrological modeling

The HL-RDHM model over the Napa River basin was calibrated based on the gridded structure HRAP (approximately 4.0 km grid size). This calibration involved refining the a priori parameters to adapt them to the local physiographic, soils and vegetative characteristics of the watersheds. This study implemented the HL-RDHM using a manual calibration method adopted from Anderson (2002). Although manual calibration can be used to track dynamic interactions in the atmosphere-land surface system, the process is complicated and highly labor-intensive. For calibration, we simultaneously used several criteria, namely hydrograph shape, peak flow, runoff volume, event start time, recession-rise turning point, and recession slope, to evaluate the simulated hydrograph; the scalar multipliers of the gridded SAC-SMA component and routing parameters were iteratively adjusted. It is not our goal to optimize calibration: instead, we calibrate only to tune the model to an acceptable condition so that the model techniques can appropriately regulate water between surface, soil, and channels to accommodate various storm situations. Once the simulated hydrographs reasonably reflect precipitation inputs and initial states in the aforementioned criteria, the manual calibration process was stopped.

In addition, Table 1 shows the calibration results for the two Napa River USGS gage stations. The calibration was implemented for a period from February to December 2011 and the results (shown in Table 1) consist of three statistics for long-term period calibration and five statistics for event-based calibration. Since the Nash-Sutcliffe, peak flow, and time to peak results were reasonable, the calibration was deemed acceptable for implementing T-year flood simulations.

3.1.2. Generation of T-year distributed precipitation fields

A storm event from 20 December, 2012 is selected as the target storm. This storm yielded total areal average precipitation of 58.3 mm for 12 h. According to NOAA Atlas 14 precipitation frequency (Table 3), the target storm represents between a 1- and 2- year

Table 1
Calibration results of the HL-RDHM.

Content	Napa R nr Napa (USGS 11458000)			Napa R nr St. Helena (USGS 11456000)		
Drainage area[mi^2]	218.0			78.8		
Obs / Sim / Diff	Obs	Sim	Diff [%]	Obs	Sim	Diff [%]
Calibration Period - Feb 2011-Dec 2011						
Long-term statistics						
Total runoff depth [m]	0.381	0.479	−25.6	0.439	0.500	−13.9
Nash-Sutcliffe	–	0.88	–	–	0.85	–
Percent bias (%)	–	−25.2	–	–	−14.4	–
Event-based statistics						
20-Mar-11						
Total runoff depth [m]	0.079	0.076	3.8	0.094	0.076	19.4
Peak flow [m^3/s]	326.3	254.8	21.9	166.4	114.0	31.5
Time to peak [hrs]	–	–	6	–	–	0
Nash-Sutcliffe	–	0.80	–	–	0.78	–
Percent bias (%)	–	4.4	–	–	18.1	–
Correlation coefficient	–	0.73	–	–	0.65	–
24-Mar-11						
Total runoff depth [m]	0.098	0.101	−3.1	0.098	0.104	−6.3
Peak flow [m^3/s]	249.3	211.0	15.3	114.4	103.4	9.6
Time to peak [hrs]	–	–	6	–	–	6
Nash-Sutcliffe	–	0.83	–	–	0.49	–
Percent bias (%)	–	−3.3	–	–	−7.3	–
Correlation coefficient	–	0.88	–	–	0.69	–

return period storm event. Fig. 6 shows hourly precipitation fields of the target storm. Observed peak flow was 371.0 m^3/s (0800 PST 24 December, 2012) at the USGS Napa station: close to a 5-year recurrence interval. The California Nevada River Forecast Center (CNRFC) issued a flood warning in response to the high flows.

There are two main reasons for selecting the 20 December, 2012 event as the target storm. Firstly, the target storm has a spatial distribution similar to that of the PRISM climate precipitation distribution. Fig. 5 shows the spatial distributions of digital elevation model (DEM), PRISM climate fields for mean annual precipitation, and 30-year mean December precipitation, and the target storm precipitation field from the MRMS QPE product (Radar-VPR-GR). This comparison showed the heaviest precipitation in the higher-elevation regions of the upper Napa River basin. The correlation coefficients of the spatial distributions for the target storm precipitation field with annual average precipitation and average precipitation on December were 0.638 and 0.750 respectively. Secondly, the target storm represents a typical event during the California rainy season. Generally during the rainy season, precipitation

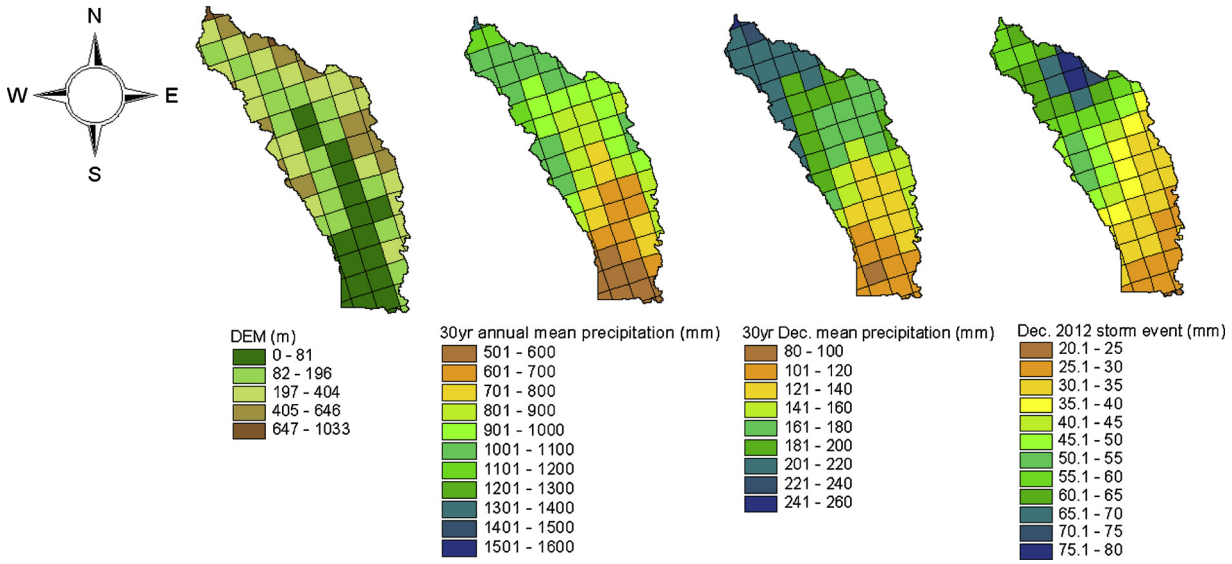

Fig. 5. Comparison of the spatial distribution features between 30-year precipitation fields from PRISM data and the selected target storm fields from MRMS QPE product. In this figure, the left panel is Digital Elevation Model (DEM), the two panels in middle are the PRISM data, and the right panel is the MRMS QPE product.

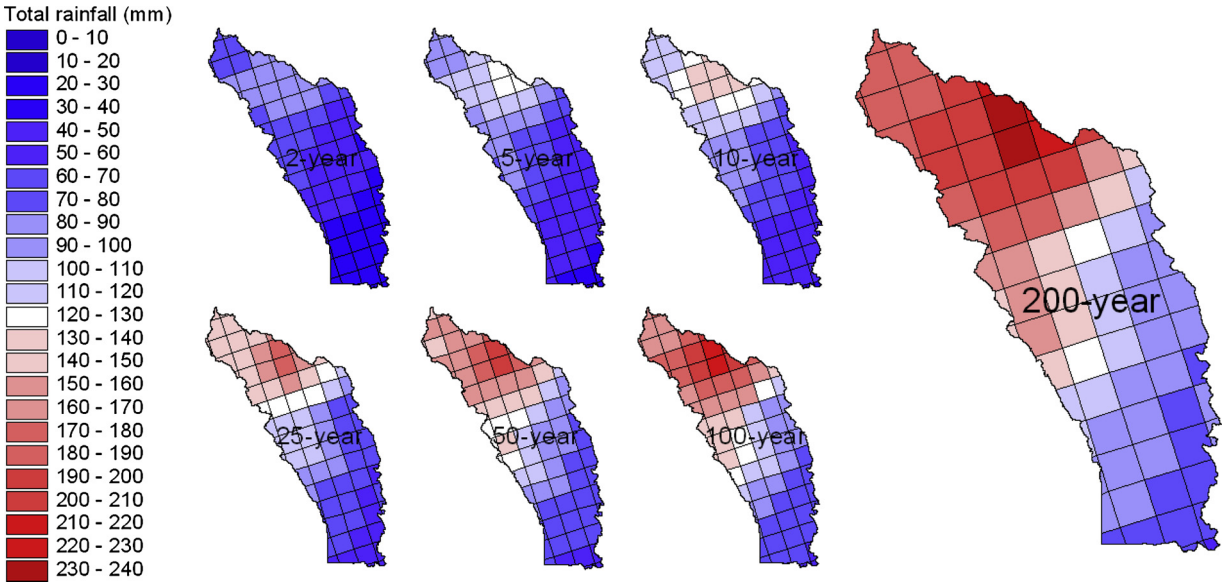

Fig. 6. Accumulated T-year distributed precipitation fields corresponding to 2 ~ 200 year return periods.

ranging from 406.4 mm to 558.8 mm, which is 80% of annual average precipitation, occurs in the Napa River basin. This study confirmed that the primary water vapor of the target storm event was created in the Pacific Ocean and came through San Francisco Bay area which is a common route water vapor comes into. Due to the complex terrain of the Napa River basin, the target storm event showed convective precipitation which is generally more intense, and of shorter duration, than stratiform precipitation. This is a reason for the heaviest precipitation in the higher-elevation regions of the application basin. According to the historical record at the USGS Napa station, most of annual maximum peak flows are recorded during this period.

The temporal distribution was extracted from the target storm to reflect a consistent time distribution to all the T-year distributed precipitation fields, and is then identified according to theory established by Huff (1967), who suggested four (first, second, third, and fourth) quartile storms of time distribution of a storm depending on a point of the time for a peak depth of precipitation. According to Huff (1967), the time distribution of the target storm is defined as the third quartile storm which has a peak at the third quartile.

2 ~ 200-year distributed precipitation derived from the radar-based precipitation fields and T-year precipitation through the merging approach were generated as shown in Fig. 6. The spatial distribution of the precipitation fields is consistent, but the QPE represent different amounts depending on the T-year return periods.

3.1.3. Estimation of antecedent moisture content states

This pre-processing step focuses on estimating and defining the states of AMC from various storm events. The five state variables (UZTWC, UZFWC, LZTWC, LZFSC, and LZFPC) analogous to soil moisture contents in the SAC-SMC model are used to estimate and define AMC states. Fig. 7 shows the maximum capacity of the five state variables across the Napa River basin. In terms of spatial variability, state variables in the upper zone represent a more homogeneous pattern than those in the lower zone. The coefficients of variation across the application basin are UZTWC: 0.264, UZFWC: 0.310, LZTWC: 0.518, LZFSC: 0.477, and LZFPC: 0.470. Soil moisture capacities in the lower zone are higher along stream channels. On an areal average basis, the lower zone capacity (231.0 mm) is over twice that of the upper zone (109.5 mm). In a comparison result of the capacities between tension and free waters, it was found that the tension water capacity naturally plays a more dominant role in retaining water than free water capacity in both zones, as the free water is easily moved by gravity.

Fourteen storm events were used to estimate AMC states, using simulations from the calibrated HL-RDHM. Table 2 shows the estimation results of AMC (mm), soil saturation (%), and fraction (%) of total soil moisture content, for each of the conceptual soil moisture storages. In the estimation results, the states of AMC are binned into three categories: dry, normal, and wet. Among the fourteen cases, Event#10 is the driest case, Event#05 represents the normal case, and Event#03 is the wettest case. In the driest case, total AMC is 21.8 mm, corresponding to 6.1% saturation. According to the two surface weather stations (St. Helena and Napa hospital) located in the Napa River basin, there had been no rain for five days prior, with only intermittent antecedent precipitation totaling 20.3 mm for the previous 30 days, which means the AMC state at the time was a moderately dry condition. On the other hand, the wettest case was derived from a complex storm generating two or more peak flows, yielding a total AMC of 184.8 mm, or 51.4% saturation, which is 8.5 times more saturated than the driest case. Additionally, the total AMC in the normal case, which is close to average conditions among the fourteen cases, is 89.9 mm, or 23.3% saturation.

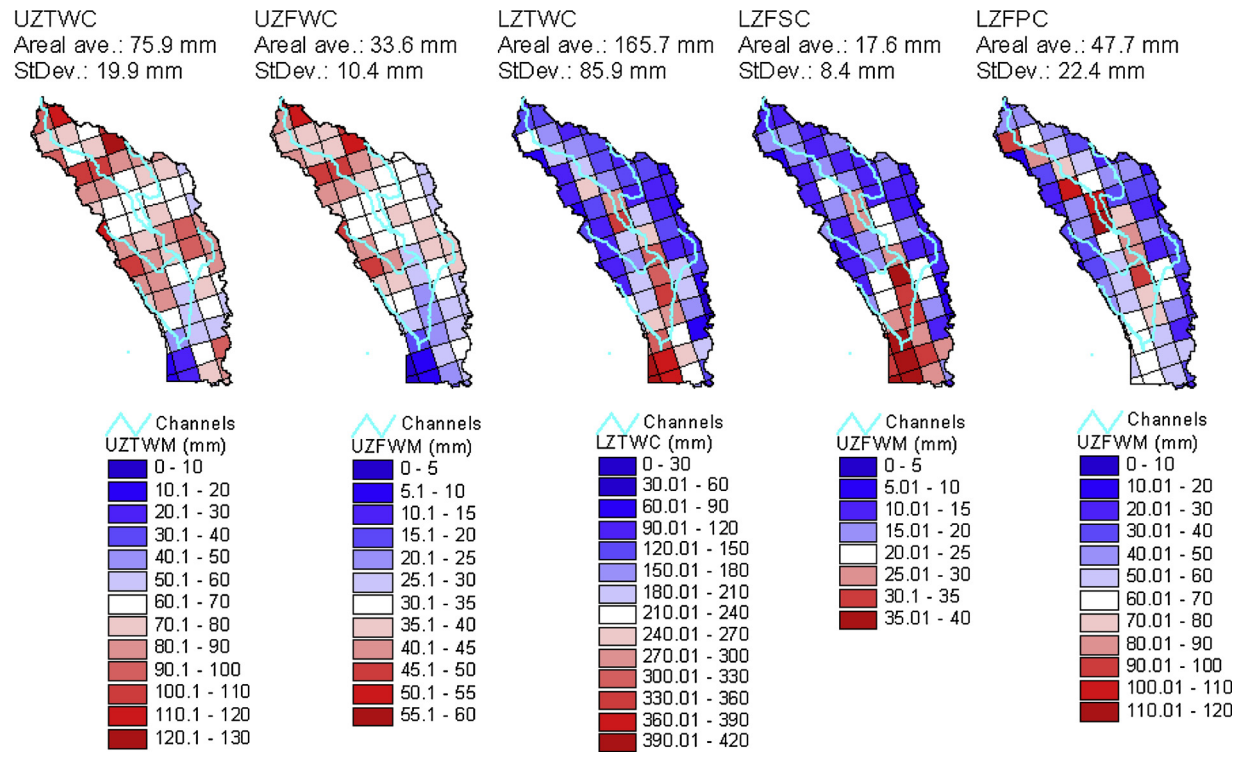

Fig. 7. Maximum capacities of five soil moisture contents in SAC-SMC Model in Napa River basin. In the figure, 'Areal ave.' is the areal average value and 'StDev.' is the standard deviation.

3.2. Assessment of effects on total runoff flow

To examine the effects of precipitation and AMC on flood frequency, total runoff flows (TRF) and peak flows simulated from a variety of T-year distributed precipitation fields and AMC states were used. The TRF (expressed as an areal average depth) was used to review the variability of total runoff volume, and the peak flow was used to derive the relation of FF-AMC-PF. In the AMC states, the minimum (21.8 mm) and maximum (184.8 mm) values indicate the driest and the wettest cases of AMC respectively, and the normal state is 83.3 mm corresponding to 23.2% saturation. In this section, the three representative AMC states and 2- and 200-year precipitation ranges were mainly used to analyze the results as mentioned above.

Table 3 and Fig. 8 show the results of the TRFs simulated with T-year precipitation and AMC states. The TRFs were simulated to a range from 20.3 mm (in the case of 2-year precipitation and the driest state) to 252.9 mm (in the case of 200-year precipitation and the wettest state).

Notable is the contribution of AMC to runoff flows when AMC states exceed a specific threshold. In some cases TRFs are generated with more than the actual total amount of precipitation, even when accounting for the initial loss of the precipitation. In the wettest case, for example, the runoff coefficients range from 1.80 to 2.13, indicating contributions of the AMC to TRFs. The results were found when exceeding 23.1% (normal AMC) of soil saturation. There are three cases, 3, 7, and 14, that are more saturated than the normal state. This translates to the soil water leading to higher TRF as the soil had been retaining enough water to produce surface run off or the water was already running off. When a complex storm with two or more independent precipitation pulses occurs in a short interval and antecedent precipitation has saturated the soil, this result is realizable as the first precipitation infiltrated into the soil could flow out together with the second precipitation pulse. However, since the runoff coefficient cannot exceed 1.0, generally, it should be noted that the results are based on the procedures established in this study. Technically, the AMC states, which is a boundary condition, and the target event are independent, and the boundary condition may have enough amount of water which could flow out as a baseflow, especially in the wet cases. This is a part of this study to maximize the effect of the AMC states on runoff flows.

To assess the effect of different AMC states on TRFs, the TRFs simulated for the same precipitation condition were compared. In the case of 2-year precipitation, for example, the TRF from the driest state is 34% of total precipitation, while the TRF from the wettest state is 202.9% of total precipitation. The difference between the two TRFs is 106.8 mm larger than 25-year precipitation amount in depth (104.4 mm referring to Table 3). This result means that the driest state of AMC absorbs roughly 33.4 mm, or 56.0% of total precipitation, assuming a 10% initial loss of total precipitation. On the other hand, the wettest AMC state contributed 74.4 mm to the TRF, assuming total precipitation (after initial loss) was completely drained out. The other results showed the same effect as this 2-year precipitation case.

Table 2
Antecedent moisture contents estimated from fourteen storm events. In this table, 'SAT (%)' is the saturation percentage and 'FRA (%)' is the fraction of total AMC.

No.	Date (mm/dd/yy HH:MM)	Indices	UZTWC (75.9)	UZFWC (33.6)	LZTWC (165.7)	LZFSC (17.6)	LZFPC (47.7)	Total (340.5)	State
1	03/13/2012 01:00	AMC (mm)	25.1	0.0	34.9	7.1	0.3	67.5	Dry
		SAT (%)	33.5	0.0	19.4	37.2	0.6	18.8	
		FRA (%)	37.2	0.0	51.7	10.5	0.4	100.0	
2	03/27/2012 01:00	AMC (mm)	64.7	1.4	98.6	11.3	8.0	184.0	Wet
		SAT (%)	86.4	4.2	54.7	59.4	15.2	51.2	
		FRA (%)	35.2	0.8	53.6	6.1	4.3	100.0	
3	03/27/2012 06:00	AMC (mm)	63.4	1.1	101.2	11.1	8.0	184.8	Wettest
		SAT (%)	84.6	3.5	56.2	58.1	15.2	51.4	
		FRA (%)	34.3	0.6	54.8	6.0	4.3	100.0	
4	11/16/2012 01:00	AMC (mm)	25.8	0.0	1.0	4.1	0.0	31.0	Dry
		SAT (%)	34.4	0.0	0.6	21.6	0.1	8.6	
		FRA (%)	83.2	0.0	3.2	13.2	0.0	100.0	
5	11/28/2012 01:00	AMC (mm)	51.2	0.0	24.2	5.6	2.9	83.9	Normal
		SAT (%)	68.4	0.1	13.4	29.3	5.6	23.3	
		FRA (%)	61.0	0.0	28.8	6.7	3.5	100.0	
6	11/28/2012 06:00	AMC (mm)	50.6	0.0	24.3	5.6	2.8	83.3	Normal
		SAT (%)	67.5	0.1	13.5	29.3	5.4	23.2	
		FRA (%)	60.7	0.0	29.2	6.7	3.4	100.0	
7	12/20/2012 13:00	AMC (mm)	51.4	0.1	98.2	11.0	4.0	164.7	Wet
		SAT (%)	68.6	0.4	54.5	57.8	7.6	45.8	
		FRA (%)	31.2	0.1	59.6	6.7	2.4	100.0	
8	02/07/2014 13:00	AMC (mm)	47.8	0.0	0.1	2.3	0.0	50.3	Dry
		SAT (%)	63.9	0.0	0.1	12.0	0.0	14.0	
		FRA (%)	95.0	0.0	0.2	4.6	0.0	100.0	
9	02/07/2014 18:00	AMC (mm)	50.9	0.1	0.1	2.3	0.0	53.4	Dry
		SAT (%)	68.0	0.2	0.1	12.1	0.0	14.9	
		FRA (%)	95.3	0.2	0.2	4.3	0.0	100.0	
10	11/19/2014 02:00	AMC (mm)	18.3	0.0	0.2	3.2	0.0	21.8	Driest
		SAT (%)	24.5	0.0	0.1	16.8	0.0	6.1	
		FRA (%)	83.9	0.0	0.9	14.7	0.0	100.0	
11	11/28/2014 17:00	AMC (mm)	45.8	0.0	6.3	3.5	0.9	56.5	Dry
		SAT (%)	61.2	0.0	3.5	18.2	1.7	15.7	
		FRA (%)	81.1	0.0	11.2	6.2	1.6	100.0	
12	11/28/2014 18:00	AMC (mm)	45.9	0.0	6.3	3.5	0.9	56.6	Dry
		SAT (%)	61.3	0.0	3.5	18.4	1.7	15.7	
		FRA (%)	81.1	0.0	11.1	6.2	1.6	100.0	
13	12/04/2014 22:00	AMC (mm)	73.8	5.8	62.0	8.6	14.2	164.4	Wet
		SAT (%)	98.5	17.4	34.4	45.2	27.1	45.7	
		FRA (%)	44.9	3.5	37.7	5.2	8.6	100.0	
14	12/05/2014 00:00	AMC (mm)	73.8	5.9	62.8	8.7	14.3	165.4	Wet
		SAT (%)	98.5	17.7	34.9	45.4	27.3	46.0	
		FRA (%)	44.6	3.6	38.0	5.3	8.6	100.0	
Standard deviation		AMC (mm)	17.0	2.1	39.7	3.3	5.1	60.6	–
		SAT (%)	22.7	6.3	22.1	17.5	9.8	16.8	–
Average		AMC (mm)	49.2	1.0	37.2	6.3	4.0	97.7	–
		SAT (%)	65.7	3.1	20.6	32.9	7.7	27.2	–

Table 3
Results of total runoff flow in depth depending on T-year return periods of precipitation and the states of AMC.

Event	AMC, mm (SAT, %)	Precipitation frequency, T-year (total amount, mm)							
		2-yr (59.7)	5-yr (75.6)	10-yr (88.0)	25-yr (104.4)	50-yr (116.6)	100-yr (128.5)	200-yr (140.5)	Max.-Min.
1	67.5 (18.8)	33.8	45.5	56.4	72.8	86.1	100.0	114.6	80.8
3	184.8 (51.4)	127.1	150.3	169.2	194.4	213.8	233.2	252.9	125.8
4	31.0 (8.6)	23.1	30.9	38.3	49.6	59.4	70.0	81.4	58.3
6	83.3 (23.2)	46.5	59.2	70.7	87.4	100.6	114.5	129.2	82.7
7	164.7 (45.8)	112.4	136.0	154.7	179.6	198.5	217.4	236.5	124.1
9	53.4 (14.9)	33.2	43.4	52.6	66.1	77.7	89.9	102.6	69.4
10	21.8 (6.1)	20.3	27.5	34.2	44.9	53.8	63.6	74.4	54.1
12	56.6 (15.7)	32.4	42.5	51.9	66.0	77.7	90.0	102.9	70.5
14	165.4 (46.0)	108.5	128.0	144.3	166.4	183.3	200.3	217.9	109.4
Max.-Min.		106.8	122.8	135.0	149.5	160.0	169.6	178.5	–

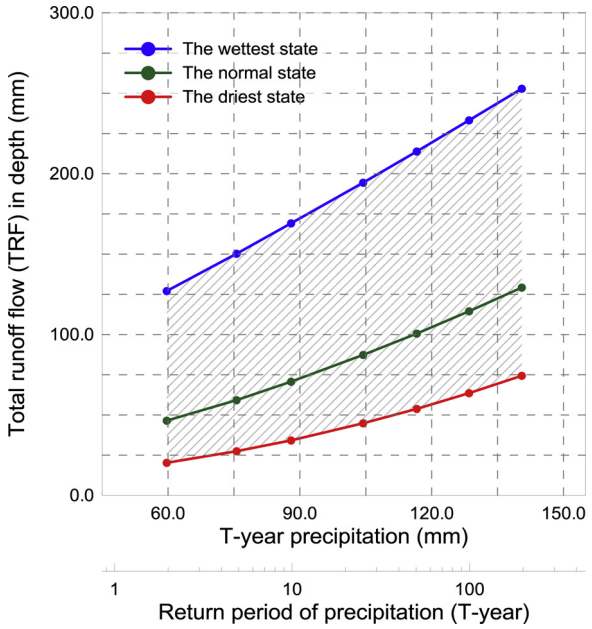

Fig. 8. Derived relation of TRF-AMC-PF.

In addition, even for a 200-year precipitation return period, for example, the TRF in the driest case is lower than that arising from a 2-year precipitation event with the wettest AMC state (see Fig. 8). Additionally, in the case of the normal AMC state, the 10-year precipitation TRF is similar to the 200-year precipitation TRF under the driest AMC. Considering the extremes, the maximum TRF (200-year precipitation / wettest AMC state) is a factor of 12.5 times the minimum TRF (2-year precipitation / driest AMC state).

How TRFs changed for the same AMC state was examined for 2- and 200-year precipitation magnitudes. For the driest AMC state, the TRF difference between 2- and 200-year precipitation events is 54.1 mm. For the wettest AMC state, the difference is 125.8 mm. This result suggests that variability of precipitation under the wettest AMC state has a larger effect on the TRF than under the driest. Fig. 9 shows an incremental trend of the TRFs (Y-axis) by precipitation increments (X-axis) and linear regression lines to analyze the trend of the increment. The precipitation and TRF increments are calculated for each T-year precipitation event relative to the 2-year precipitation event. The effect of the precipitation magnitude on TRF is nearly linear (linear regression lines have R-squared values of 0.99). With saturated soil, precipitation magnitude has a large effect on the TRF since the regression line slope of the wettest AMC state (slope = 0.63) is steeper than that for the driest AMC state (slope = 0.46).

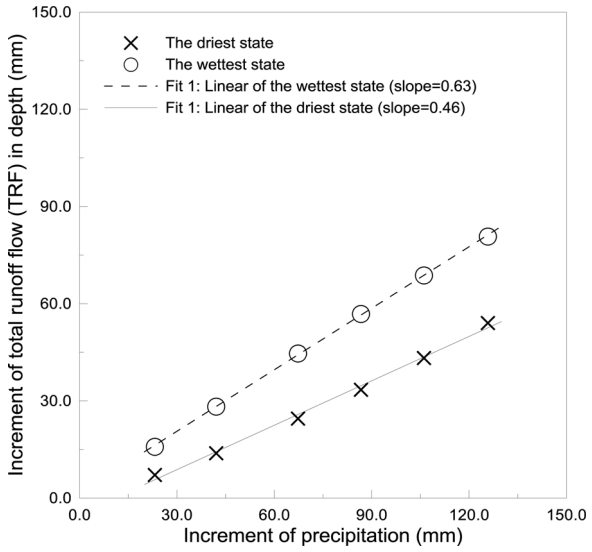

Fig. 9. Increment trend of total runoff flow and precipitation. The symbols from left to right indicate 2 ~ 200-year return periods.

Table 4
Results of peak flow depending on T-year return periods of precipitation and the states of AMC.

Event	AMC, mm (SAT, %)	Precipitation frequency, T-year (total amount, mm)						
		2-yr (59.7)	5-yr (75.6)	10-yr (88.0)	25-yr (104.4)	50-yr (116.6)	100-yr (128.5)	200-yr (140.5)
1	67.5	4543	7732	11,036	16,901	21,906	27,378	33,359
	(18.8)	(1.5)	(2.5)	(4.1)	(9.8)	(20.6)	(46.7)	(113.9)
3	184.8	19,155	28,038	35,688	46,262	54,533	63,171	71,964
	(51.4)	(13.7)	(51.5)	(161.2)	(780.8)	(< 1000)	(< 1000)	(< 1000)
4	31.0	2841	4876	7034	10,621	13,915	17,903	22,408
	(8.6)	(1.2)	(1.6)	(2.2)	(3.8)	(6.3)	(11.3)	(22.2)
6	83.3	6406	10,201	14,094	20,339	25,548	31,034	37,190
	(23.2)	(2.0)	(3.6)	(6.4)	(16.3)	(35.5)	(80.5)	(201.7)
7	164.7	17,936	26,953	34,588	45,073	53,561	61,694	70,677
	(45.8)	(11.4)	(43.8)	(136.8)	(653.9)	(< 1000)	(< 1000)	(< 1000)
9	53.4	4174	7066	9932	14,366	18,618	23,505	28,808
	(14.9)	(1.5)	(2.3)	(3.5)	(6.7)	(12.6)	(26.2)	(57.8)
10	21.8	2424	4270	6198	9516	12,435	15,897	19,982
	(6.1)	(1.1)	(1.5)	(2.0)	(3.2)	(5.0)	(8.4)	(15.5)
12	56.6	4158	6976	9847	14,627	19,035	23,844	29,186
	(15.7)	(1.5)	(2.2)	(3.4)	(7.0)	(13.4)	(27.5)	(61.1)
14	165.4	14,129	21,173	27,508	36,342	43,503	50,442	58,192
	(46.0)	(6.5)	(18.5)	(47.6)	(177.7)	(517.3)	(< 1000)	(< 1000)

3.3. Assessment of effects on peak flow

Simulated peak flows, their T-year return periods and the forcing precipitation and AMC states are tabulated in Table 4. Clearly, peak flow varies considerably with precipitation and AMC. In the table, the range of peak flow is from 68.6 to 2037.8 m^3/s, corresponding to a range from 1.1-year to over 1000-year recurrence intervals.

For a given precipitation condition, simulated peak flows differ significantly, depending on AMC state. For 2-year return periods for precipitation, maximum peak flow (542.4 m^3/s, corresponding to a 13.7-year flow) is 7.9 times than minimum peak flow (68.6 m^3/s, corresponding to a 1.1-year flow). In terms of flood frequency, the maximum return period is 12.5 times the minimum return period. For the 200-year return period for precipitation, maximum peak flow (2037.8 m^3/s, corresponding to a > 1000-year flow) is 3.6 times the minimum peak flow (565.8 m^3/s, corresponding to a 15.5-year flow). In terms of flood frequency, the maximum return period is at least 64.5 times the minimum.

Depending on precipitation magnitudes, simulated peak flows also vary significantly for a given AMC state. In the driest AMC state, maximum peak flow is 8.2 times the minimum. In terms of flood frequency, the maximum return period is 14.1 times the minimum. In the wettest AMC state, maximum peak flow is 3.8 times the minimum. In terms of flood frequency, the maximum return period is over 73.0 times the minimum.

Table 4 shows an interesting contrast in runoff characteristics between events #7 (45.8% saturation) and #14 (46.0% saturation). Despite an almost negligible difference in the degree of saturation (0.2%), but the peak flow for event #7 is 1.24 times that of event #14. In both cases, tension water dominates the soil water retention, but the water content in the upper and lower zones are different. In Event#7, lower zone tension water is around twice the upper zone tension water (see Table 4). However, in the case of Event#14, the tension water content in both of zones is similar (upper zone tension water is 73.8 mm, the lower zone tension water is 62.8 mm). Though these results are determined by complicated hydrological processes, antecedent precipitation, and climatic features during days with no rain, it is clear that the state of total AMC plays a significant role in generating peak flows and moisture contents in soil layers.

Fig. 10 shows how peak flows (Y-axis) change with the states of AMC (the top X-axis is a degree of saturation, the bottom is AMC in depth), specifically demonstrating the effect of AMC state on peak flows from different precipitation conditions (2- and 200-year recurrence intervals). Exponential and linear regression lines fitted to the peak flow responses to the state of AMC demonstrate that peak flows increase considerably with increasing AMC states in both of the 2- and 200-year precipitation cases. R-squared values of the exponential and linear regression lines exceed 0.96. The regression lines are comparable in terms of statistics: the linear regression lines, for example, show that the impact of AMC on peak flows is obviously different depending on the precipitation magnitudes since the slope of linear regression line resulted from 200-year precipitation is roughly 3 times the 2-year precipitation case. Similar to the case of the TRF relationship, this indicates peak flows could be more sensitive to precipitation magnitudes when the soil is saturated.

Peak flows estimated from hydrologic frequency analysis (FFA-Flood) and simulated from distributed hydrologic modeling (DHM-Flood) in this study are compared in Fig. 11. FFA-Flood is a set of peak flows corresponding to 2 ~ 200-year return periods of flood as tabulated in Table 4. DHM-Flood is a set of peak flows simulated using 2 ~ 200-year precipitation fields and the states of AMC. There are several interesting issues to discuss; (1) the relation of the FFA-Flood and the DHM-Flood, (2) the effect of the state of AMC on the relation of the FFA-Flood and the DHM-Flood, and (3) whether the DHM-Flood approach can properly simulate the FFA-Floods. The

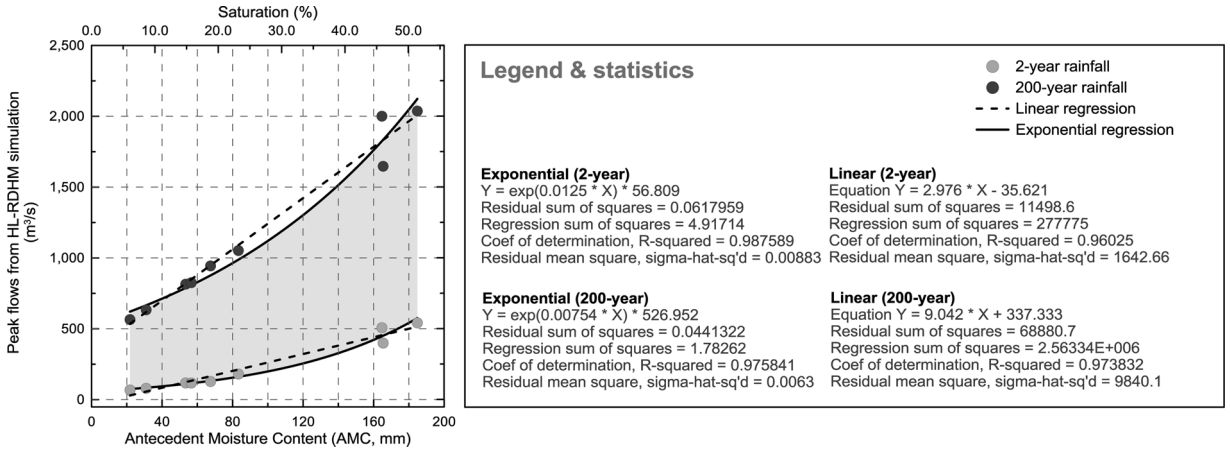

Fig. 10. Relation of AMC and peak flow depending on 2- and 200- year precipitations.

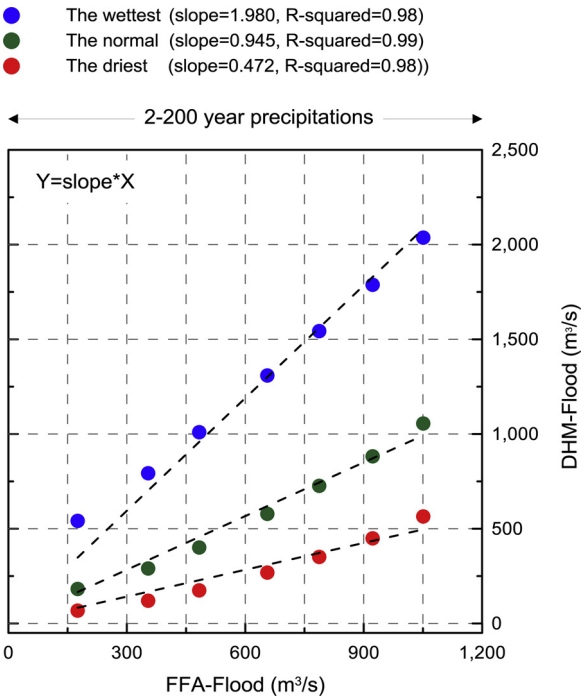

Fig. 11. Comparison of USGS T-year floods based on flood frequency analysis and the simulated T-year floods based on 2 ~ 200-year distributed precipitations and the normal state of AMC.

issues can be addressed by first considering whether T-year precipitation can generate identical return periods of FFA-Flood. Also, it was found that the relation of T-year FFA-Floods and DHM-Floods are nearly linear, as the R-squared ranges from 0.98 to 0.99. The regression lines are naturally moving up and down by the states of AMC. The slopes of the wettest, the normal, and the driest states are 1.98, 0.94, and 0.47 respectively. This result indicates that the effect of the AMC states has a larger effect on the relation as the AMC state is getting saturated (issue 2 above).

Regarding the third issue, it was possible to simulate nearly identical FFA-Floods using the normal state of AMC. DHM-Floods from the normal state of AMC are quite similar with the FFA-Floods. In Fig. 14, the scatter points of peak flows between FFA-Flood and DHM-Flood from the normal state are remarkably close to Y = X, and the linear regression line has R-squared value 0.99 which is enough to regard the relation of FFA-Flood and DHM-Flood as linear. This result indicates that T-year precipitation fields can generate peak flows corresponding to nearly identical recurrence intervals of flood through adopting the normal state of AMC as a boundary condition for the T-year flood simulation process using the hydrologic model. Thus, we could define the normal AMC condition of approximately 23.3% saturation as the standard state of AMC which could simulate T-year floods by using corresponding return periods of precipitation.

Fig. 12 shows the relation of precipitation frequency (PF), the state of AMC, and flood frequency. It contains the potentially

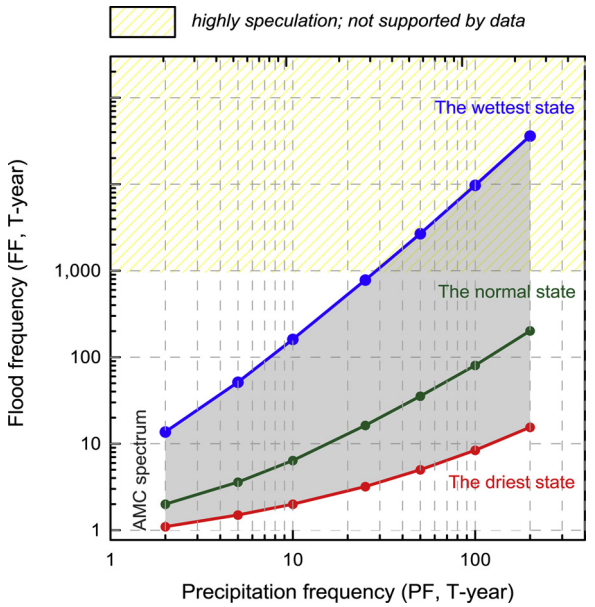

Fig. 12. Derived relation of FF-AMC-PF.

feasible range of flood frequency by PF and AMC. This figure consists of three lines representing each relation depending on the three states of AMC. The range of flooding return periods was considerable depending on the states of AMC and the PFs. In the driest state of AMC, 1.1 ~ 15.5-year flood could be generated, and in the wettest state of AMC, 13.7 ~ over 1000-year flood could be generated by the PFs. A remarkable feature in this result is that 200-year precipitation in the driest state can generate only a peak flow corresponding to 21-year recurrence interval, which demonstrates that the state of AMC has a large effect on flood frequency. In the case of the normal state of AMC, however, T-year precipitation yielded approximately the same T-year return period of flood. In the wettest state of AMC, only 5-year precipitation could generate a 50 + -year flood event.

4. Discussion and conclusions

This study assessed the effects of antecedent moisture condition on flood frequency using the HL-RDHM distributed hydrologic model forced with T-year distributed precipitation data under a range of AMC states. This study described the need of pre-processings to generate the T-year distributed precipitations and to estimate the AMC states. The assessment was conducted in terms of reviewing the relations among TRF-AMC-PF and FF-AMC-PF to focus on the effect of precipitation magnitudes and AMC states on discharge. However, we have several assumptions which might generate uncertainties, and it should be shared with readers and for future works. The methodology used in this study is for smaller watersheds whose AMC states and precipitation magnitudes are primary drivers to occur extreme floods. Also, it is for specific watersheds with no upstream regulation and no effects of snow on streamflows. The HL-RDHM used in this study was calibrated using the observed streamflow data, while the SAC-SMA model was not calibrated as the application area has no soil moisture observation sensors. According to the calibration results described in the chapter 3.2, the results showed the acceptable statistics of the simulated hydrographs against to the observed data, but it should be noted that the estimated soil moisture contents might have bias compared to true values as the fact could occur systematic errors of the SAC-SMA state variables.

Understanding uncertainties in the rainfall-runoff modelling needs for meaningful quantification of the results (Beven, 1993; Pappenberger and Beven, 2006). Since the HL-RDHM used in this study is one of rainfall-runoff models, potential uncertainties due to hydrological modelling should be discussed in this chapter. In general, the uncertainties may arise from the model structure (Butts et al., 2004), parameterization process (Etter et al., 2018), and boundary conditions (Pappenberger et al., 2006). Especially, the parameterization process depends on how many observation points and long data record are used to calibrate a model for a watershed matter (Etter et al., 2018). In this study, two streamflow observation points were used to calibrate and verify the model, but soil moisture variables were not verified due to the absent of soil moisture monitoring system in the application watershed. The soil moisture variables (e.g. volumetric soil moisture contents such as an amount of free and tension waters) are important to derive direct runoff flows which determine a magnitude and timing of peak flows in hydrological modeling. Considering the comments from previous studies and the study procedure, it should be noted that the results could be slightly varied with hydrologic models and calibration conditions. However, it is speculated that the uncertainties will be not big enough to change the results and conclusions below.

In addition, this study is an experimental-regional study and has a hypothesis and constraint: (a) This study assumed the application basin as a small/medium category size whose antecedent soil moisture states and precipitation magnitudes are main drivers

to occur extreme floods. Thus, artificial effects (e.g. dam operation) on estimating flood frequency is excluded. (b) Since this study is implemented using a target storm event which has specific features, the results might be varied in features of an applied target storm event, especially a duration period. Based on these hypothesis, constraint, and methodology, the conclusions are described as follows:

The maximum TRF for the 200-year precipitation and wettest AMC state is 12.5 times the minimum TRF for 2-year precipitation and driest AMC state. For wetter-than-normal AMC states, TRFs were generating more runoff than the total precipitation amount due to the soil already running off or retaining enough water to run off. Such cases are likely in a complex storm event with multiple pulses of precipitation. We found that the relation of the precipitation magnitude on TRF is nearly linear. Given the constraints of this study, overall results demonstrate that the effect of AMC state is larger than precipitation magnitude on TRFs.

The relation of FFA-Flood and DHM-Flood based on the normal state of AMC were remarkably close to 1:1 meaning that the relation of FFA-Flood and DHM-Flood is interchangeable. This result suggests that when AMC is near normal, a 100-year precipitation event could generate a peak flow corresponding to approximately the 100-year flood frequency. Thus, we could define the normal state to the standard state of AMC which can simulate T-year FFA-Floods by using hydrologic modeling with corresponding T-year precipitation inputs.

The AMC state has a large effect on flood frequency, demonstrated by the fact that a 200-year precipitation event in the driest AMC state generates a peak flow only corresponding to a 15.5-year recurrence interval. Also, a 10-year precipitation event in the wettest AMC state could generate a > 150-year flow. Based on our results, in the study region, a rainy season with a saturated soil condition, a roughly 7-year precipitation event could trigger an extreme flood event with over a > 100-year return period. On the other hand, a 200-year precipitation event could generate around a 15-year flood event during a dry season with drier-than-normal soils.

In conclusion, this study derived the relations of FF-AMC-PF, and confirmed the considerable effects of AMC and precipitation and their interaction on flood discharge in T-year recurrence intervals. It is expected that this analysis could be applied to many flood-related areas. In terms of hydrological analysis of flood, the relations could be used to assess contributions of AMC state and precipitation magnitude to flood frequency thresholds for rainy and dry seasons. Using the relations and predicted precipitation, we are able to estimate predicted flood intensity to a T-year return period. Finally, the importance of soil moisture to flood runoff should be emphasized: clearly, soil moisture monitoring could aid in improving flood forecasting.

Declaration of Competing Interest

None.

Acknowledgements

This work was supported by the California Department of Water Resources and the NOAA Physical Sciences Division. We appreciate the internal reviewer contribution from Mike Hobbins.

Appendix A. Supplementary data

Supplementary material related to this article can be found, in the online version, at doi:https://doi.org/10.1016/j.ejrh.2019.100629.

References

Anderson, E., 2002. Calibration of Conceptual Hydrologic Models for Use in River Forecasting. National Weather Service / Office of Hydrologic Development 392pp.
Arnell, N.W., Gosling, S.N., 2016. The impacts of climate change on river flood risk at the global scale. Clim. Change 134, 387–401. https://doi.org/10.1007/s10584-014-1084-5.
Beven, K.J., 1993. Prophesy, reality and uncertainty in distributed hydrological modelling. Adv Water Resour. 16, 41–51. https://doi.org/10.1016/0309-1708(93)90028-E.
Blazkova, S., Beven, K.J., 2002. Flood frequency estimation by continuous simulation for a catchment treated as ungauged (with uncertainty). Water Resour. Res. 38, 1–14. https://doi.org/10.1029/2001WR000500.
Brath, A., Montanari, A., Moretti, G., 2006. Assessing the effect on flood frequency of land use change via hydrological simulation (with uncertainty). J. Hydrol. 324, 141–153. https://doi.org/10.1016/j.jhydrol.2005.10.001.
Bergstrôm, S., Harlin, J., Lindstorm, G., 1993. Spillway design floods in Sweden: I. New guidelines. Hydrol. Sci. J. 37, 505–519. https://doi.org/10.1080/02626669209492615.
Butts, M.B., Payne, J.T., Kristensen, M., Madsen, H., 2004. An evaluation of the impact of model structure and complexity on hydrologic modelling uncertainty for streamflow prediction. J. of Hydrol. 298, 242–266. https://doi.org/10.1016/j.jhydrol.2004.03.042.
Cameron, D., Beven, K., Naden, P., 2000. Flood frequency estimation by continuous simulation under climate change (with uncertainty). Hydrol. Earth Syst. Sci. 4, 393–405. https://doi.org/10.5194/hess-4-393-2000.
Cameron, D., Beven, K.J., Tawn, J., Blazkova, S., Naden, P., 1999. Flood frequency estimation by continuous simulation for a gauged upland catchment (with uncertainty). J. Hydrol. 219, 169–187. https://doi.org/10.1016/S0022-1694(99)00057-8.
Castillo, V.M., Gómez-Pñaza, A., Martínez-Mena, M., 2003. The role of antecedent soil water content in the runoff response of semiarid catchments: a simulation approach. J. Hydrol. 284, 114–130. https://doi.org/10.1016/S0022-1694(03)00264-6.
Chifflard, P., Kranl, J., zur Strassen, G., Zepp, H., 2018. The significance of soil moisture in forecasting characteristics of flood events. A statistical analysis in two nested catchments. J. Hydrol. Hydromech. 66 (1), 1–11. https://doi.org/10.1515/johh-2017-0037.
Chow, V.T., Maidment, D.R., Mays, L.W., 1988. Applied Hydrology. McGraw Hill.
Dalrymple, T., 1960. Flood-frequency analyses, U.S. Geological Survey Water-Supply Paper 1543-A, Report.
De Michele, C., Salvadori, G., 2002. On the derived flood frequency distribution: analytical formulation and the influence of antecedent soil moisture condition. J.

Hydrol. 262, 245–258. https://doi.org/10.1016/S0022-1694(02)00025-2.
De Michele, C., Rosso, R., 2001. Uncertainty assessment of regionalized flood frequency estimates. J. Hydrol. Eng. 6, 453–459. https://doi.org/10.1061/(ASCE)1084-0699(2001)6:6(453).
De Paola, F., Ranucci, A., Feo, A., 2013. Antecedent moisture condition (SCS) frequency assessment: A case study in southern Italy. Irrig. Drain 62, 61–71. https://doi.org/10.1002/ird.1801.
Eagleson, P.S., 1972. Dynamics of flood frequency. Water Resour. Res. 8, 878–898. https://doi.org/10.1029/WR008i004p00878.
England Jr., J.F., Cohn, T.A., Faber, B.A., Stedinger, J.R., Thomas Jr., W.O., Veilleux, A.G., Kiang, J.E., Mason Jr., R.R., 2018. Guidelines for Determining Flood Flow Frequency—Bulletin 17C: U.S. Geological Survey Techniques and Methods. book 4, chap. B5, 148 p.. https://doi.org/10.3133/tm4B5.
Etter, S., Strobl, B., Seibert, J., van Meerveld, H.J.I., 2018. Value of uncertain streamflow observations for hydrological modelling. Hydrol. Earth Syst. Sci. 22, 5243–5257. https://doi.org/10.5194/hess-22-5243-2018.
Gotvald, A.J., Barth, N.A., Veilleux, A.G., Parrett, C., 2012. Methods for Determining Magnitude and Frequency of Floods in California, based on Data Through Water Year 2006. Scientific Investigations Rep. 2012-5113. U.S. Dept. of the Interior, U.S. Geological Survey, Reston, VA.
Gumbel, E.J., 1941. The return period of flood flows. Ann. Math. Stat. 12, 163–190. https://projecteuclid.org/euclid.aoms/1177731747.
Halbert, K., Nguyen, C., Payrastre, O., Gaume, E., 2016. Reducing uncertainty in flood frequency analyses: a comparison of local and regional approaches involving information on extreme historical floods. J. Hydrol. 541, 90–98. http://wwwsciencedirect.com/science/article/pii/S0022169416000342.
Han, H., Kim, J., Chandrasekar, V., Choi, J., Lim, S., 2019. Modeling streamflow enhanced by precipitation from atmospheric river using the NOAA national water modela case study of the Russian river basin for February 2004. Atmosphere 10 (8 (February)). https://doi.org/10.3390/atmos10080466.
Hawkins, R.H., Hjelmfelt, A.T., Zevenberger, A.W., 1985. Runoff probability, storm depth, and curve numbers. J. Irrig. Drain. Eng. ASCE 111, 330–340. https://doi.org/10.1061/(ASCE)0733-9437(1985)111:4(330).
Hollis, G.E., 1975. The effect of urbanization on floods of different recurrence interval. Water Resour. Res. 11, 431–435. https://doi.org/10.1029/WR011i003p00431.
Huff, F.A., 1967. Time distribution of rainfall in heavy storms. Water Resour. Res. 11, 889–896. https://doi.org/10.1029/WR003i004p01007.
Huza, J., Teuling, A.J., Braud, I., Grazioli, J., Melsen, L.A., Nord, G., Raupach, T.H., Uijlenhoet, R., 2014. Precipitation, soil moisture and runoff variability in a small river catchment (Ardèche, France) during HyMeX Special Observation Period 1. J. Hydrol. 516, 330–342. https://doi.org/10.1016/j.jhydrol.2014.01.041.
Javelle, P., Fouchier, C., Arnaud, P., Lavabre, J., 2010. Flash flood warning at ungauged locations using radar rainfall and antecedent soil moisture estimations. J. Hydrol. 394, 267–274. https://doi.org/10.1016/j.jhydrol.2010.03.032.
Johnson, L.E., Hsu, C., Zamora, R., Cifelli, R., 2016. Assessment and Applications of Distributed Hydrologic Model - Russian-Napa River Basins, CA. NOAA Technical Memorandum PSD-316, NOAA Printing Office, Silver Spring, MD. https://doi.org/10.7289/V5M32SS9. 101 pp.
Katz, R.W., Parlange, M.B., Naveau, P., 2002. Statistics of extremes in hydrology. Adv. Water Resour. 25, 1287–1304. https://doi.org/10.1016/S0309-1708(02)00056-8.
Kay, A.L., Davies, H.N., Bell, V.A., Jones, R.G., 2009. Comparison of uncertainty sources for climate change impacts: flood frequency in England. Clim. Change 92, 41–63. https://doi.org/10.1007/s10584-008-9471-4.
Kim, J., Yoo, C., 2014. Use of a dual Kalman filter for real-time correction of mean field bias of radar rain rate. J. Hydrol. 519, 2785–2796. https://doi.org/10.1016/j.jhydrol.2014.09.072.
Kim, J., Yoo, C., Lim, S., Choi, J., 2015. Usefulness of relay-information-transfer for radar QPE. J. Hydrol. 531, 308–319. https://doi.org/10.1016/j.jhydrol.2015.07.006.
Kim, J., Johnson, L.E., Cifelli, R., Choi, J., Chandrasekar, V., 2018a. Derivation of soil moisture recovery relation using Soil Conservation Service (SCS) curve number method. Water 10 (7), 833. https://doi.org/10.3390/w10070833.
Kim, J., Johnson, L.E., Cifelli, R., Coleman, T., Herdman, L., Martyr-Koller, R., Finzi-Hart, J., Erikson, L., Barnard, P.L., 2018b. San Francisco Bay Integrated Flood Forecasting Project Summary Report; NOAA Technical Memorandum PSD-317. NOAA Printing Office: Silver Spring, MD, USA.
Klemeš, V., 2006. Hydrological and engineering relevance of flood frequency analysis. Hydrologic Frequency Modeling. pp. 1–18. https://doi.org/10.1007/978-94-009-3953-0_1.
Koren, V., Reed, S., Smith, M., Zhang, Z., Seo, D.-J., 2004. Hydrology laboratory research modeling system (HL-RMS) of the US national weather service. J. Hydrol. 291, 297–318. https://doi.org/10.1016/j.jhydrol.2003.12.039.
Koren, V., Smith, M., Duan, Q., et al., 2003. Use of a priori parameter estimates in the derivation of spatially consistent parameter sets of rainfall–runoff models. Calibration of watershed models. In: In: Duan, Q. (Ed.), Water Science and Application Series Vol. 6. Amer. Geophys. Union, pp. 239–254. https://doi.org/10.1002/9781118665671.ch18.
Krajewski, W.F., Lakshimi, V., Georgakakos, K.P., Jain, S.J., 1991. A Monte Carlo study of rainfall sampling effect on a distributed catchment model. Water Resour. Res. 27, 119–128. https://doi.org/10.1029/90WR01977.
Martínez-Mena, M., Albaladejo, J., Castillo, V., 1998. Factors influencing surface runoff generation in a Mediterranean semi-arid environment: Chicamo watershed, SE Spain. Hydrol. Process. 12, 741–754. https://doi.org/10.1002/(SICI)1099-1085(19980430)12:5<741::AID-HYP622>3.0.CO;2-F.
Merz, B., Plate, E.J., 1997. An analysis of the effects of spatial variability of soil and soil moisture on runoff. Water Resour. Res. 33, 2909–2922. https://doi.org/10.1029/97WR02204.
Merz, R., Blöschl, G., 2008a. Flood frequency hydrology. 1: temporal, spatial and causal expansion of information. Water Resour. Res. 44 (8). https://doi.org/10.1029/2007WR006744. W08432.
Merz, R., Bloschl, G., 2008b. Flood frequency hydrology. 2: combining data evidence. Water Resour. Res. 44https://doi.org/10.1029/2007WR006745. W08433.
National Weather Service (NWS), 2011. Hydrology Laboratory-Research Distributed Hydrologic Model (HL-RDHM) User Manual, Version 3.2.0. NWS Report. pp. 131.
Osborn, H.B., Hickok, R.B., 1968. Variability of rainfall affecting runoff from a semiarid rangeland watershed. Water Resour. Res. 4, 199–203. https://doi.org/10.1029/WR004i001p00199.
Ouarda, T.B.M.J., Girard, C., Cavadias, G.S., Bobee, B., 2001. Regional flood frequency estimation with canonical correlation analysis. J. Hydrol. 254, 157–173. https://doi.org/10.1016/S0022-1694(01)00488-7.
Pappenberger, F., Beven, K.J., 2006. Ignorance is bliss: Or seven reasons not to use uncertainty analysis. Water Resour. Res. 42, 1–8. https://doi.org/10.1029/2005WR004820.
Pappenberger, F., Matgen, P., Beven, K.J., Henry, J.B., Pfister, L., de Fraipont, P., 2006. Influence of uncertain boundary conditions and model structure on flood inundation predictions. Adv. Water Resour. 29, 1430–1449. https://doi.org/10.1016/j.advwatres.2005.11.012.
Pandey, G.R., Nguyen, V.T.V., 1999. A comparative study of regression based methods in regional flood frequency analysis. J. Hydrol. 225, 92–101. https://doi.org/10.1016/S0022-1694(99)00135-3.
Penna, D., Tromp-van Meerveld, H.J., Gobbi, A., Borga, M., Dalla Fontana, G., 2011. The influence of soil moisture on threshold runoff generation processes in an Alpine headwater catchment. Hydrol. Earth Syst. Sci. 15, 689–702. https://doi.org/10.5194/hess-15-689-2011.
Perica, S., Dietz, S., Heim, S., Hiner, L., Maitaria, K., Martin, D., Pavlovic, S., Roy, I., Trypaluk, C., Unruh, D., Yan, D., Yekta, M., Zhao, T., Bonnin, G., Brewer, D., Chen, L., Parzybok, T., Yarchoan, J., 2014. NOAA Atlas 14: Precipitation-Frequency Atlas of the United States. Volume 6 Version 2.3: California, report.
Powell, R.W., 1943. A simple method of estimating flood frequencies. Civil Eng. 13 (2), 105–106.
Prosdocimi, I., Kjeldsen, T.R., Miller, J.D., 2015. Detection and attribution of urbanization effect on flood extremes using nonstationary flood-frequency models. Water Resour. Res. 51, 4244–4262. https://doi.org/10.1002/2015WR017065.
Smith, A., Sampson, C., Bates, P., 2015. Regional flood frequency analysis at the global scale. Water Resour. Res. 51, 539–553. https://doi.org/10.1002/2014WR015814.
Sorooshian, S., Duan, Q., Gupta, V.K., 1993. Calibration of rainfall-runoff models: application of global optimization to the Sacramento soil moisture accounting model. Water Resour. Res. 29, 1185–1194. https://doi.org/10.1029/92WR02617.
Spies, R.R., Franz, K.J., Hogue, T.S., Bowman, A.L., 2015. Distributed hydrologic modeling using satellite-derived potential evapotranspiration. J. Hydrometeorol. 16, 129–146. https://doi.org/10.1175/JHM-D-14-0047.1.

Thorstensen, A., Nguyen, P., Hsu, K., Sorooshian, S., 2016. Using densely distributed soil moisture observations for calibration of a hydrologic model. J. Hydrometeorol. 17, 571–590. https://doi.org/10.1175/JHM-D-15-0071.1.

Tramblay, Y., Bouvier, C., Martin, C., Didon-Lescot, J.F., Todorovik, D., Domergue, J.M., 2010. Assessment of initial soil moisture conditions for event-based rainfall-runoff modelling. J. Hydrol. 380, 305–317. https://doi.org/10.1016/j.jhydrol.2010.04.006.

Tucker, G.E., Bras, R.L., 2000. A stochastic approach to modeling the role of rainfall variability in drainage basin evolution. Water Resour. Res. 36, 1953–1964. https://doi.org/10.1029/2000WR900065.

Willie, D., Chen, H., Chandrasekar, V., Cifelli, R., 2016. Evaluation of multisensor quantitative precipitation estimation in Russian river basin. J. Hydrol. Eng. 22, 1–11. https://doi.org/10.1061/(ASCE)HE.1943-5584.0001422.

Yoo, C., Park, C., Yoon, J., Kim, J., 2013. Interpretation of mean-field bias correction of radar rain rate using the concept of linear regression. Hydrol. Process. 28, 5081–5092. https://doi.org/10.1002/hyp.9972.

Yoo, C., Kim, J., Yoon, J., 2012. Uncertainty of areal average rainfall and its effect on runoff simulation: a case study for the Chungju Dam basin. Korea. J. Civ. Eng. KSCE 16, 1085–1092. https://doi.org/10.1007/s12205-012-1646-x.

Zhang, H., Wang, Y., Wang, Y., Lu, D., Wang, W., 2013. Quantitative comparison of semi- and fully-distributed hydrologic models in simulating flood hydrographs on a mountain watershed in southwest China. J. Hydrodynam. 25, 877–885. https://doi.org/10.1016/S1001-6058(13)60436-9.

Zhang, J., et al., 2016. Multi-Radar Multi-Sensor (MRMS) quantitative precipitation estimation: initial operating capabilities. Bull. Am. Meteor. Soc. 97, 621–638. https://doi.org/10.1175/BAMS-D-14-00174.1.